Journal of Engineering Mathematics **23**: 95–117, 1989.

Wave-interference effects on a truncated cylinder in a channel

R.W. YEUNG[1] and S.H. SPHAIER[2]
[1] *Department of Naval Architecture and Offshore Engineering, University of California, Berkeley, CA 94720, U.S.A.*; [2] *School of Post-graduate Engineering (COPPE), Federal University of Rio de Janeiro, Rio de Janeiro, 21945, Brazil*

Received 21 September 1988; accepted 7 December 1988

Abstract. The effects of channel walls on the hydrodynamic properties of a floating vertical cylinder are examined. An interior eigensolution under the cylinder is matched with an exterior eigensolution in a manner similar to Yeung [1]. Wave effects due to an image cylinder can be conveniently expressed in terms of the coordinates of the central cylinder by the use of Graff's theorem. The infinite array results in a slowly convergent series which has to be summed with caution. Results for the heave added mass and damping of a cylinder for several geometric configurations are obtained. Also presented in the paper are results for the diffraction of incident waves about the same cylinder. The channel walls exert an important influence on the radiation and diffraction properties, the latter to a lesser extent. Such influence is characterized by the presence of "spikes" at wave frequencies corresponding to the occurrence of symmetric transverse resonant modes in the channel. An analytical solution of a three-dimensional flapper wavemaker given in the Appendix further confirms such characteristics. In the high-frequency range, the radiation properties approach those of a single cylinder. In the low-frequency limit, they exhibit a behavior similar to that of a two-dimensional horizontal cylinder heaving in water of finite depth.

1. Introduction

The evaluation of hydrodynamic coefficients for bodies oscillating near a free surface plays an important role in the study of their behavior in the sea. More recently, there has been an increase of interest in studying hydrodynamic interference effects among bodies [2, 3, 4]. Such interests stem from the fact that many offshore structures or wave-energy extractors are made of a collection of identical geometrical components. Interference effects are also of practical concern when excessively large models are tested in wave tanks of relatively limited width [5]. Finally, in performing numerical computations, it is not unusual to simulate laterally unbounded flow by truncating the fluid domain with channel walls [6]. Some theoretical understanding of the hydrodynamic interference caused by imaging effects of the channel walls is thus highly desirable.

This paper examines the hydrodynamic characteristics of a single body placed in an *infinite* array of its own images. For simplicity, we have chosen to study a vertical (floating) cylinder of finite draft. Its radiation properties for heaving motion are obtained as a function of frequency and the relevant geometric parameters. Also solved here is the complementary problem of wave diffraction about this cylinder in an array configuration. This particular body geometry for the case of *laterally unbounded water* was solved by Garrett [7] for wave diffraction and by Yeung [1] for wave radiation. The method of matched eigenfunction expansions used therein reduced the problem to the numerical solution of an infinite system. Such a quasi-analytical treatment has been used subsequently with success by Miao and Liu [8], McIver [9] and Kagemoto and Yue [10] in a variety of related contexts. The present

problem of an infinite array can be tackled using the same approach by exploiting Graff's addition theorem [11] to relate the coordinates of one cylinder to another. Spring and Monkmeyer [12] have considered the transverse exciting force on a bottom-mounted cylinder, with attention directed to the confinement effects of the tank walls. A similar investigation was carried out recently by Matsui et al. [13] for the overturning moment. However, radiation and diffraction properties of a finite-draft body showing the effects of channel walls are not available in the literature at present.

The present treatment of the array-interaction problem uses a direct solution method, in which the coefficients of N circumferential modes and K vertical modes for each cylinder are determined concurrently. Previously, a multiple-scattering technique has been used by Twersky [14] and Simon [12], the latter with further simplification using a "plane-wave" approximation. Such an approximation enables one to use the single-cylinder results but requires the use of the assumption of large spacing to wave-length ratio. Our present procedure does not contain this restriction but requires a careful treatment of a slowly convergent Hankel series. Interference effects caused by nonpropagating modes of neighboring cylinders are neglected in our model. This error can be shown to be exponentially small.

As will be shown, the hydrodynamic properties of the cylinder in a channel are characterized by the presence of a sequence of "spiky responses", at which the far-field behavior from the cylinder is associated with the occurrence of transverse waves sloshing in the channel. In the neighborhood of these so-called "cut-off frequencies", the added mass and damping coefficients have a square-root singular behavior just below and just above the cut-off, respectively. The low-frequency behavior of the heave added mass and damping for a single cylinder in finite water-depth was discussed in considerable detail by Yeung [1]. Based on the arguments used therein, it can be deduced that the hydrodynamic coefficients for the present problem will have behavior similar to those of a *two-dimensional* heaving cylinder in finite-depth water [15, 16], and will transform gradually to those of a single cylinder [1] as the width of the channel increases. These basic features are borne out in the numerical results.

2. The mathematical model

To describe the fluid motion induced by the presence of a cylinder of radius a located on the centerline of a channel of width w, we choose a cylindrical coordinate system (r_0, θ_0, z) centered at the axis of the cylinder. Referring to Fig. 1, we consider first a Cartesian coordinate system with origin O at the still water level, the Oz axis coinciding with the axis of the cylinder and pointing upwards, the Ox axis located in the longitudinal plane of symmetry of the channel, and the Oy axis perpendicular to the channel walls. A point in the fluid defined by position vector $\mathbf{R}$ will therefore have a cylindrical radius r_0 given by $\sqrt{x^2 + y^2}$ and a cylindrical angle given by θ_0. The bottom of the channel coincides with the plane $z = -h$ while the bottom of the cylinder is on the plane $z = -d$.

2.1. Heaving vertical cylinder of finite draft

Under the assumptions that the fluid is incompressible, the flow irrotational, and the heave amplitude small compared with the cylinder radius, the fluid motion at time t can be described

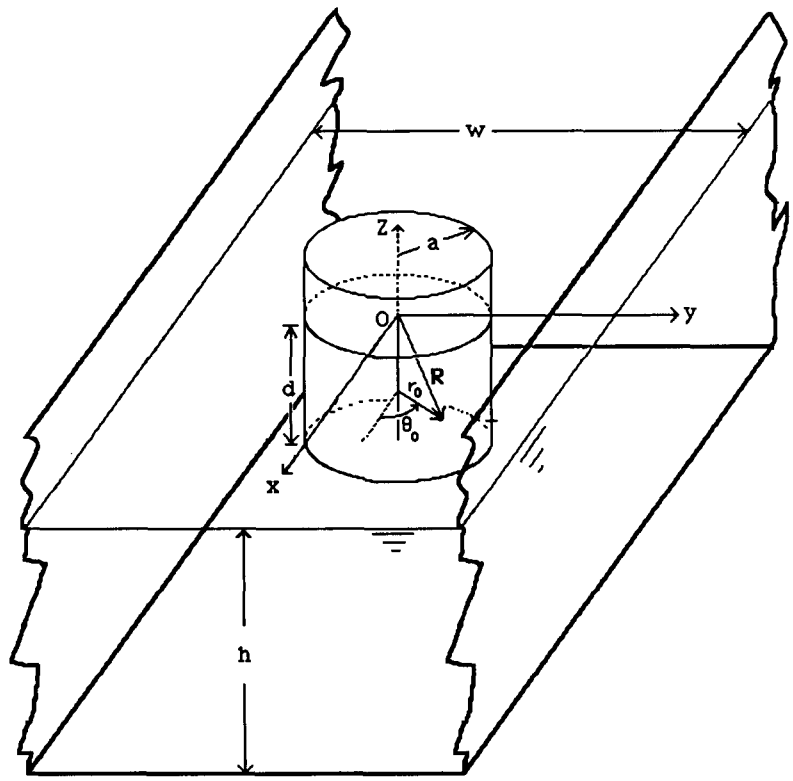

Fig. 1. Coordinate systems and nomenclature.

by the potential function

$$\phi = \mathrm{Re}\,[-\mathrm{i}\sigma\varphi(r_0, \theta_0, z)\zeta_3 \mathrm{e}^{-\mathrm{i}\sigma t}], \tag{2.1}$$

where ζ_3 and σ are the amplitude and angular frequency of the heave motion respectively. Here i represents the imaginary unit associated with time. The spatial potential $\varphi(r_0, \theta_0, z)$ satisfies the following linear boundary-value problem:

$$\nabla^2\varphi = 0 \qquad \text{in the fluid,} \tag{2.2}$$

$$\frac{\partial\varphi}{\partial z} - \nu\varphi = 0 \qquad \text{at } z = 0, \tag{2.3}$$

$$\frac{\partial\varphi}{\partial z} = 0 \qquad \text{at } z = -h, \tag{2.4}$$

$$\frac{\partial\varphi}{\partial z} = 1 \qquad \text{at } z = -d, \quad r_0 < a, \tag{2.5}$$

$$\frac{\partial \varphi}{\partial r_0} = 0 \qquad \text{at } -d < z < 0, \quad r_0 = a, \tag{2.6}$$

$$\frac{\partial \varphi}{\partial y} = 0 \qquad \text{at } y = \pm w/2, \tag{2.7}$$

where $\nu = \sigma^2/g$ is a frequency parameter, and g the gravitational acceleration.

By the method of images, the present problem is equivalent to one with an infinite array of parallel cylinders having their vertical axes all in a plane perpendicular to the channel walls. Each cylinder in this array is separated by a distance w. For the j-th cylinder, we define local coordinates r_j and θ_j as shown in Fig. 2. Following Yeung [1], we divide the fluid domain into two regions, an interior one under the central cylinder and a exterior one surrounding the central cylinder. The potential function in the interior region is defined by $\varphi^{(i)}$ and in the exterior region by $\varphi^{(e)}$. The interior potential $\varphi^{(i)}$ must satisfy

$$\nabla^2 \varphi^{(i)} = 0 \qquad \text{in the fluid,} \tag{2.8}$$

$$\frac{\partial \varphi^{(i)}}{\partial z} = 0 \qquad \text{at } z = -h, \quad 0 < r_0 < a, \tag{2.9}$$

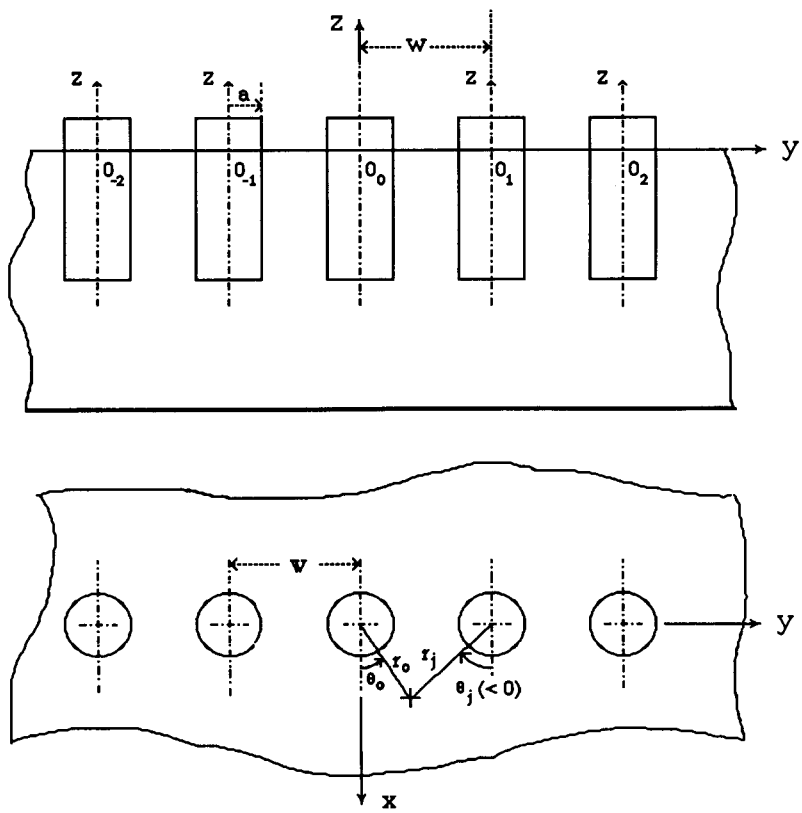

Fig. 2. Central cylinder and image cylinders.

$$\frac{\partial \varphi^{(i)}}{\partial z} = 1 \qquad \text{at } z = -d, \quad 0 < r_0 < a, \tag{2.10}$$

$$\varphi^{(i)} = \varphi^{(e)} \qquad \text{at } r_0 = a, \quad -d < z < 0. \tag{2.11}$$

The exterior potential $\varphi^{(e)}$ must satisfy

$$\nabla^2 \varphi^{(e)} = 0 \qquad \text{in the fluid,} \tag{2.12}$$

$$\frac{\partial \varphi^{(e)}}{\partial z} - \nu \varphi^{(e)} = 0 \qquad \text{at } z = 0, \tag{2.13}$$

$$\frac{\partial \varphi^{(e)}}{\partial z} = 0 \qquad \text{at } z = -h, \tag{2.14}$$

$$\frac{\partial \varphi^{(e)}}{\partial y} = 0 \qquad \text{at } y = \pm w/2. \tag{2.15}$$

Further, we have

$$\frac{\partial \varphi^{(e)}}{\partial r_0} = \frac{\partial \varphi^{(i)}}{\partial r_0} \qquad \text{at } r_0 = a, \quad -h < z < -d, \tag{2.16}$$

$$\frac{\partial \varphi^{(e)}}{\partial r_0} = 0 \qquad \text{at } r_0 = a, \quad -d < z < 0. \tag{2.17}$$

Conditions (2.11) and (2.16) ensure continuity of the potential and its radial derivative on the virtual boundary shared by the two domains. Finally, a radiation condition must be imposed which states that propagating disturbances must be outgoing.

The interior solution can be written as the sum of a homogeneous solution $\varphi_h^{(i)}$ and a particular solution $\varphi_p^{(i)}$:

$$\varphi^{(i)} = \varphi_h^{(i)} + \varphi_p^{(i)}. \tag{2.18}$$

The particular solution $\varphi_p^{(i)}$ is given by Yeung [1]:

$$\varphi_p^{(i)} = \frac{1}{2(h-d)}\left[(z+h)^2 - \frac{r_0^2}{2}\right]. \tag{2.19}$$

Separation of variables in cylindrical coordinates yields the following homogeneous solution:

$$\varphi_h^{(i)} = \sum_{n=0}^{\infty} \varepsilon_n \cos(2n\theta_0) \left\{ \frac{A_{0n}}{4} \left(\frac{r}{a}\right)^{2n} + \sum_{k=1}^{\infty} \frac{A_{kn}}{2} Z_k^{(i)} \frac{I_{2n}(\lambda_k r_0)}{I_{2n}(\lambda_k a)} \right\}, \tag{2.20a}$$

$$Z_k^{(i)}(\lambda_k z) = \cos[\lambda_k(z+h)], \quad \lambda_k = \frac{k\pi}{h-d}, \tag{2.20b}$$

with the coefficients A_{kn} to be determined. Here ε_n is the Jacobi index, $\varepsilon_n = 1$ for $n = 0$; $\varepsilon_n = 2$ for $n > 0$, and I_{2n} is the modified Bessel function of the first kind, order $2n$. The non-axisymmetric modes ($n \neq 0$) are used here to account for interference effects caused by the image cylinders. Only circumferential modes of even multiples of n exist because of symmetry about the Ox and Oy axes.

Similarly, the general exterior solution $\varphi^{(e)}$, satisfying (2.12)–(2.15) and the radiation condition, can be shown to be

$$\varphi^{(e)} = \sum_{j=-\infty}^{\infty} \sum_{n=0}^{\infty} \sum_{k=0}^{\infty} a_{kn}^{j} \frac{\varepsilon_n}{2} \frac{R_{2n}(m_k r_j)}{R_{2n}(m_k a)} Z_k^{(e)}(m_k z) \cos(2n\theta_j), \tag{2.21a}$$

where the radial modes R_{2n} and vertical modes $Z_k^{(e)}$ are given by

$$R_{2n}(m_k r_j) = \begin{cases} H_{2n}^{(1)}(m_0 r_j) & \text{for } k = 0, \\ K_{2n}(m_k r_j) & \text{for } k \neq 0; \end{cases}$$

$$Z_k^{(e)}(m_k z) = \begin{cases} \cosh[m_0(z + h)]/N_0^{1/2} & \text{for } k = 0, \\ \cos[m_k(z + h)]/N_k^{1/2} & \text{for } k \neq 0; \end{cases} \tag{2.21b}$$

$$N_0 = [\sinh(2m_0 h) + 2m_0 h]/(4m_0 h), \quad N_k = [\sin(2m_k h) + 2m_k h]/(4m_k h), \quad k > 0.$$

The eigenvalues m_k are the solutions of

$$m \tanh(mh) = \nu, \tag{2.22}$$

where m represents m_0 for $k = 0$, or im_k for $k \neq 0$. In (2.21b), $H_{2n}^{(1)}$ is the Hankel function of the first kind, order $2n$, which yields outgoing disturbances and K_{2n} is the MacDonald function of order $2n$. Note that (2.21a) is expressed in terms of the cylindrical coordinates of each of the cylinders, $-\infty < j < \infty$. The coefficients of the exterior series a_{kn}^{j} are identical for all j. The term associated with $j = 0$ in (2.21a) represents the potential due to the central cylinder $\varphi_0^{(e)}$; the terms associated with $j \neq 0$ describe the influence generated by all other cylinders, which we denote by $\varphi_{\text{int}}^{(e)}$. In order to apply the boundary condition (2.16–17) on the central cylinder, we express the (r_j, θ_j), $j \neq 0$, in terms of (r_0, θ_0) by using Graff's Addition Theorem (see Watson [11]). Before proceeding with this transformation, we will take advantage of the following approximation for $\varphi_{\text{int}}^{(e)}$:

$$\varphi_{\text{int}}^{(e)} \sim \sum_{n=0}^{\infty} \varepsilon_n \frac{a_{0n}}{2} Z_0^{(e)}(m_0 z) \sum_{\substack{j=-\infty \\ j\neq 0}}^{\infty} \frac{H_{2n}^{(i)}(m_0 r_j)}{H_{2n}^{(i)}(m_0 a)} \cos(2n\theta_j) + \mathrm{O}\left(\sum_j \exp(-jm_1 w)/\sqrt{j}\right). \tag{2.23}$$

Since the leading evanescent mode is governed by a value of $m_1 h > \pi/2$, the neglected terms would be of the order $\exp(-\pi w/2h)$. Inclusion of the non-propagating modes does not complicate the theory substantially. However, they are the wave modes that are expected to contribute the primary interference effects because of their slow spatial decay rate.

In Appendix A, it is shown that $\varphi_{\text{int}}^{(e)}$ can be rewritten as

$$\varphi_{\text{int}}^{(e)} = Z_0^{(e)}(m_0 z) \sum_{n=0}^{\infty} \frac{a_{0n}}{H_{2n}^{(1)}(m_0 a)} \sum_{p=0}^{\infty} \cos(2p\theta_0) \bar{g}_{pn}(m_0 r_0), \tag{2.24}$$

where $\bar{g}_{pn} = \varepsilon_p(g_{pn} + g_{-pn})$, with

$$g_{pn} = (-1)^{n+p} J_{2p}(m_0 r_0) \sum_{j=1}^{\infty} H_{2(n+p)}^{(1)}(jm_0 w). \tag{2.25}$$

Thus, the contribution of the image cylinders is described by a series of Hankel functions whose asymptotic behavior for large arguments is oscillatory with a relatively slow decay rate. The asymptotic form of the j-series is therefore given by

$$\sum_{j=1}^{\infty} H_n^{(1)}(jx) \sim e^{-i(n(\pi/2)+(\pi/4))} \sqrt{\frac{2}{\pi x}} \sum_{j=1}^{\infty} \frac{e^{ijx}}{\sqrt{j}}. \tag{2.26}$$

This slowly convergent series was mentioned by Thomas [17]. Our treatment, which is similar to Matsui et al. [13], is detailed in Appendix B.

In summary, the complete exterior potential, expressed in terms of (r_0, θ_0, z), is given by

$$\varphi^{(e)} = \sum_{k=0}^{\infty} Z_k^{(e)}(m_k z) \sum_{n=0}^{\infty} a_{kn} U_{nk}(r_0, \theta_0), \tag{2.27}$$

where the function U_{nk} is defined as

$$U_{nk} = \begin{cases} \dfrac{1}{H_{2n}^{(1)}(m_0 a)} \left\{ \dfrac{\varepsilon_n}{2} H_{2n}^{(1)}(m_0 r_0) \cos(2n\theta_0) + \displaystyle\sum_{j=0}^{\infty} \bar{g}_{jn} \cos(2j\theta_0) \right\} & \text{for } k = 0, \\ \dfrac{\varepsilon_n}{2} \dfrac{K_{2n}(m_k r_0)}{K_{2n}(m_k a)} \cos(2n\theta_0) & \text{for } k \neq 0. \end{cases} \tag{2.28}$$

2.2. Determination of the coefficients A_{kn} and a_{kn}

The determination of the interior coefficients A_{kn} and exterior coefficients a_{kn} can be accomplished by applying the continuity conditions (2.11) and (2.16) on the virtual surface $\{r_0 = a; -h < z < -d\}$ and condition (2.17) for the exterior potential [1]. Let us define the operator

$$\mathscr{L}^i[f(a, \theta_0, z)] = \frac{1}{\pi(h - d)} \int_{-h}^{-d} \int_0^{\pi} f(a, \theta_0, z) Z_p^{(i)} \cos(2q\theta_0) \, d\theta_0 \, dz. \tag{2.29}$$

Applying $\mathscr{L}^i$ to (2.11) and using (2.19) and (2.20) on the left-hand side, and (2.27) on the right-hand side, we obtain

$$\tfrac{1}{4} A_{pq} = f_{pq} + \frac{1}{2} \sum_{k=0}^{K} a_{kq} \mathscr{C}_{pk} + \frac{\mathscr{C}_{p0}}{2\varepsilon_q} \sum_{n=0}^{N} \frac{a_{0n} \bar{g}_{gn}(m_0 a) \varepsilon_n}{H_{2n}^{(1)}(m_0 a)}, \quad p = 0, \ldots, K, \quad q = 0, \ldots, N \tag{2.30}$$

where f_{pq} involves the particular solution $\varphi_p^{(i)}$:

$$f_{pq} = \begin{cases} \dfrac{1}{2(h-d)}\left\{\dfrac{a^2}{2} - \dfrac{1}{3}(h^2 + d^2) + \dfrac{2hd}{3}\right\} & \text{for } p = q = 0, \\ \dfrac{(-1)^p}{(p\pi)^2}(d-h) & \text{for } p \neq 0, \quad q = 0, \\ 0 & \text{for } q \neq 0. \end{cases} \tag{2.31}$$

The A_{pq}'s, truncated as a finite set for $K + 1$ vertical modes and $N + 1$ circumferential modes, are coupled with the exterior a_{kn}'s via the $\mathscr{C}_{pk}$ defined below:

$$\mathscr{C}_{pk} = (h-d)\frac{(-1)^p}{N_k^{1/2}} \begin{cases} m_0 \sinh [m_0(h-d)]/[m_0^2(h-d)^2 + (p\pi)^2] & \text{for } k = 0, \\ m_k \sin [m_k(h-d)]/[m_k^2(h-d)^2 - (p\pi)^2] & \text{for } k \neq 0. \end{cases} \tag{2.32}$$

To impose (2.16–17), we introduce the exterior operator

$$\mathscr{L}^e [f(a, \theta_0, z)] = \frac{1}{\pi h}\int_{-h}^{0}\int_0^{\pi} f(a, \theta_0, z)\, Z_p^{(e)} \cos(2q\theta)\, \mathrm{d}\theta_0\, \mathrm{d}z. \tag{2.33}$$

Applying $\mathscr{L}^e$ to (2.16–17) by using the differentiated expressions of (2.19–20) and (2.27), we obtain

$$\begin{aligned} &\tfrac{1}{2} a_{pq} m_p \frac{R'_{2q}(m_p a)}{R_{2q}(m_p a)} + \frac{\delta_{p0}}{2\varepsilon_q}\sum_{n=0}^{N}\frac{a_{0n} m_0 \bar{g}'_{qn}}{H_{2n}^{(1)}(m_0 a)}\varepsilon_n \\ &\quad = e_{pq} + \frac{h-d}{2h}\left\{A_{0q}\mathscr{C}_{0p}\frac{q}{a} + \sum_{k=1}^{K} A_{kq}\mathscr{C}_{kp}\lambda_k \frac{I'_{2q}(\lambda_k a)}{I_{2q}(\lambda_k a)}\right\}, \\ &\qquad\qquad p = 0, \ldots, k, \quad q = 0, \ldots, N, \end{aligned} \tag{2.34}$$

where the primes indicate differentiation with respect to the argument of the function; δ_{pq} is the Kronecker delta and

$$e_{pq} = \mathscr{L}^e\left[\frac{\partial \varphi_p^{(i)}}{\partial r_0}\right] = \begin{cases} \dfrac{a \sinh [m_0(h-d)]}{2(d-h)N_0^{1/2} m_0 h} & \text{for } p = q = 0, \\ \dfrac{a \sin [m_p(h-d)]}{2(d-h)N_p^{1/2} m_p h} & \text{for } p \neq 0, \quad q = 0, \\ 0 & \text{for } q \neq 0. \end{cases} \tag{2.35}$$

The solution of linearly coupled systems (2.30) and (2.34) yields the values of the unknown coefficients A_{kn} and $a_{kn} (k = 0, \ldots, K, n = 0, \ldots, N)$. To solve these equations, we treat the A_{kn}, a_{kn}, f_{kn} and e_{kn} as vectors **A**, **a**, **f**, and **e** respectively. The coefficient matrices

multiplying **A** and **a** on the right-hand side of (2.30) and (2.34) can be designated as **C1**, **C2**, **GB**, and **DG** so that these equations can be written in the form

$$\mathbf{A} = 4\mathbf{f} + \mathbf{C1} * \mathbf{a} + \mathbf{GB} * \mathbf{a}, \tag{2.36a}$$

$$\mathbf{a} = 2\mathbf{e} + \mathbf{C2} * \mathbf{A} - \mathbf{DG} * \mathbf{a}. \tag{2.36b}$$

Substituting (2.36a) in (2.36b) we can solve for **a** and then using (2.36a) we can recover **A**. In actual computations common terms in the coefficient matrices are saved to avoid redundant computations.

With the coefficients A_{kn} and a_{kn} now known in (2.20) and (2.24), we can determine the hydrodynamic pressure acting on the cylinder. A straight-forward integration leads to the following formulas for the (non-dimensional) heave added mass $\bar{\mu}_{33}$ and the damping coefficient $\bar{\lambda}_{33}$:

$$\bar{\mu}_{33} + \mathrm{i}\bar{\lambda}_{33} = \frac{1}{\varrho\pi a^3}\left[\mu_{33} + \frac{\mathrm{i}}{\sigma}\lambda_{33}\right] = \frac{h-d}{2a} - \frac{a}{8(h-d)} + \left\{\frac{A_{00}}{4a} + \sum_{k=1}^{K}(-1)^k \frac{A_{k0}}{a^2}\frac{I_0'(\lambda_k a)}{\lambda_k I_0(\lambda_k a)}\right\}, \tag{2.37}$$

where we note that only the axisymmetric mode ($n = 0$) contributes to the final expression.

2.3. Diffraction around multiple cylinders

The solution of the diffraction problem can be obtained in a way similar to that of the heave problem. Three modifications of the procedure in Sec. 2.1 are necessary: (a) an incident wave potential φ_0 must be added to the external potential in (2.21a); (b) the internal boundary-value problem is now homogeneous, thus $\varphi_p^{(i)} = 0$ in (2.18); (c) since the centerplane of the channel is the only plane of symmetry, the series in (2.20a) and (2.21a) must have $2n$ replaced by n to include odd values of circumferential modes.

The potential of a plane wave of amplitude ζ_0 propagating along the x-axis is given by

$$\phi_{\mathrm{inc}}(r_0, \theta_0, z, t) = \mathrm{Re}\,[\sigma\zeta_0 h\varphi_0(r_0, \theta_0, z)\mathrm{e}^{-\mathrm{i}\sigma t}], \tag{2.38}$$

where it is well known that the spatial component φ_0 can be expressed as

$$\varphi_0 = \frac{-\cosh\,[m_0(z+h)]}{m_0 h \sinh\,(m_0 h)} \sum_{m=0}^{\infty} \varepsilon_m (\mathrm{i})^{m+1} J_m(m_0 r_0)\cos\,(m\theta_0). \tag{2.39}$$

The external potential, by analogy to (2.27), can be written as

$$\varphi^{(e)} = \varphi_0 + \sum_{k=0}^{\infty} Z_k^{(e)}(m_k z) \sum_{n=0}^{\infty} \frac{a_{kn}\varepsilon_n R_n(m_k r_0)\cos\,(n\theta_0)}{2R_n(m_k a)} + Z_0^{(e)}(m_0 z) \sum_{n=0}^{\infty} \frac{a_{0n}\varepsilon_n}{2H_n^{(1)}(m_0 a)} \sum_{p=0}^{\infty} \cos\,(p\theta_0)\bar{g}_{pn}(m_0 r_0) \tag{2.40}$$

with $\bar{g}_{pn}$ still defined by (2.25), but g_{pn} now given by

$$g_{pn} = J_p(m_0 r_0)\cos\left[(n-p)\frac{\pi}{2}\right]\sum_{j=1}^{\infty} H_{n+p}^{(1)}(jm_0 w). \tag{2.41}$$

The internal potential is given only by a homogeneous solution:

$$\varphi^{(i)} = \sum_{n=0}^{\infty} \varepsilon_n \cos(n\theta_0)\left\{\frac{A_{0n}}{4}\left(\frac{r}{a}\right)^n + \sum_{k=1}^{\infty}\frac{A_{kn}}{2} Z_k^{(i)}\frac{I_n(\lambda_k r_0)}{I_n(\lambda_k a)}\right\}. \tag{2.42}$$

As before, applying the operator $\mathscr{L}^i$ to (2.11) and $\mathscr{L}^e$ to (2.16–17), and using the new expressions (2.40) and (2.42), we obtain

$$\tfrac{1}{4}A_{pq} = -\frac{(\mathrm{i})^{q+1}J_q(m_0 a)\mathscr{C}_{p0}N_0^{1/2}}{m_0 h \sinh(m_0 h)} + \frac{1}{2}\sum_{k=0}^{K}\mathscr{C}_{pk}a_{kq} + \frac{\mathscr{C}_{p0}}{2\varepsilon_q}\sum_{n=0}^{N}\frac{a_{0n}\bar{g}_{qn}\varepsilon_n}{H_n^{(1)}(m_0 a)},$$

$$p = 0, \ldots, K, \quad q = 0, \ldots, N, \tag{2.43}$$

and

$$-(\mathrm{i})^{q+1}\frac{J_q'(m_0 a)\delta_{p0}N_0^{1/2}}{\sinh(m_0 h)} + \frac{a_{pq}m_p h}{2}\frac{R_q'(m_p a)}{R_q(m_p a)} + \frac{\delta_{p0}m_0 h}{2\varepsilon_q}\sum_{n=0}^{N}\frac{a_{0n}\bar{g}_{qn}'\varepsilon_n}{H_n^{(1)}(m_0 a)}$$

$$= \frac{h-d}{2h}\left\{\frac{A_{0q}}{2}\mathscr{C}_{0p}\frac{q}{a} + \sum_{k=1}^{K}A_{kq}\mathscr{C}_{kp}\lambda_k\frac{I_q'(\lambda_k a)}{I_q(\lambda_k a)}\right\}, \quad p = 0, \ldots, K, \; q = 0, \ldots, N. \tag{2.44}$$

This coupled linear system can be treated in a manner similar to that described in Sec. 2.2.

With the coefficients A_{pq} and a_{pq} solved, we can use (2.40) and (2.42) to obtain wave-exciting (horizontal and vertical) forces **F** and pitching moment **M** (about O):

$$\begin{Bmatrix}\mathbf{F}\\ \mathbf{M}\end{Bmatrix}\mathrm{e}^{-\mathrm{i}\sigma t} = -\iint_{\mathscr{S}}\varrho\frac{\partial\phi}{\partial t}\begin{Bmatrix}\mathbf{n}\\ \mathbf{R}\times\mathbf{n}\end{Bmatrix}\mathrm{d}\mathscr{S}, \tag{2.45}$$

where **n** is the inward-pointing unit normal of the cylinder and $\mathscr{S}$ is the surface of the cylinder (see Fig. 1). A straight-forward integration of (2.45) yields the following *nondimensional* expressions for the exciting forces and moments:

$$\bar{F}_1 = \frac{F_1}{\varrho g\pi a^2\zeta_0} = \frac{-\mathrm{i}\nu h^2}{a}\left[\frac{2f_0 J_1(m_0 a)}{m_0 h\sinh(m_0 h)} + \sum_{k=0}^{K}\frac{a_{k1}}{N_k^{1/2}}f_k + \frac{f_0}{N_0^{1/2}}\sum_{n=0}^{N}\frac{\varepsilon_n a_{0n}\bar{g}_{1n}}{2H_n^{(1)}(m_0 a)}\right] \tag{2.46}$$

$$\bar{F}_3 = \frac{F_3}{\varrho g\pi a^2\zeta_0} = \mathrm{i}\nu h\left\{\frac{A_{00}}{4} + \frac{1}{a}\sum_{k=1}^{K}(-1)^k A_{k0}\frac{I_0'(\lambda_k a)}{\lambda_k I_0(\lambda_k a)}\right\}, \tag{2.47}$$

$$\bar{F}_5 = \frac{F_5}{\varrho g \pi a^2 \zeta_0 h} = \frac{-\mathrm{i}\nu h^2}{a}\left[\frac{2L_0 J_1(m_0 a)}{m_0 h \sinh(m_0 h)} + \sum_{k=0}^{K} \frac{L_k}{N_k^{1/2}} a_{k1} + \frac{L_0}{N_0^{1/2}} \sum_{n=1}^{N} \frac{a_{0n}\varepsilon_n}{2H_n^{(1)}(m_0 a)} \bar{g}_{1n}\right.$$

$$\left. + \frac{A_{01}}{8}\frac{a^2}{h^2} + \sum_{k=1}^{K} \frac{A_{k1}(-1)^k}{\lambda_k^2 h^2}\left\{\frac{\lambda_k a I_1'(\lambda_k a)}{I_1(\lambda_k a)} - 1\right\}\right], \tag{2.48}$$

where the auxiliary functions f_k and L_k are given by:

$$f_k(m_k d) = \begin{cases} \{\sinh(m_0 h) - \sinh[m_0(h-d)]\}/(m_0 h) & \text{for } k = 0, \\ \{\sin(m_k h) - \sin[m_k(h-d)]\}/(m_k h) & \text{for } k \neq 0; \end{cases} \tag{2.49}$$

$$L_k(m_k d) = \begin{cases} -\dfrac{\cosh(m_0 h)}{m_0^2 h^2} + \dfrac{d}{m_0 h^2}[m_0(h-d)] + \dfrac{\cosh[m_0(h-d)]}{m_0^2 h^2} & \text{for } k = 0, \\ \dfrac{\cos(m_k h)}{m_k^2 h^2} + \dfrac{d}{m_k h^2}\sin[m_k(h-d)] - \dfrac{\cos[m_k(h-d)]}{m_k^2 h^2} & \text{for } k \neq 0. \end{cases} \tag{2.50}$$

3. Numerical results

A computer code was developed based on the theories described in Sec. 2. The heave-motion problem and diffraction problem are closely related, the work involved in the conversion from the former to the latter was minimal. The code has been checked by comparing results of the present formulation with those of the following special cases: (1) a single heaving cylinder of finite draft [1], and (2) the pitch wave-exciting moment for a bottom mounted cylinder in a channel [13]. In both incidences, the agreements were excellent.

In order to obtain some insight into the behavior of the radiation properties of a body in a channel, we have also obtained the analytical solution of a three-dimensional pulsating wavemaker (see Appendix C). The flapper wavemaker hinged at $y = \pm a$ on the plane $x = 0$ (Fig. C.1) generates a flux condition similar to that of a heaving vertical cylinder, both solutions being symmetric about the plane $x = 0$. From equation (C.1), it is clear that propagating modes moving down the channel that are of wave number α_{0n} exist only if the following criterion is met:

$$\left(\frac{\alpha_{0n}}{m_0}\right)^2 = 1 - \left(\frac{n\pi}{m_0 w}\right)^2 > 0, \tag{3.1}$$

where m_0 is the wave number given by (2.22). Here n is associated with the modal variation across the width of the channel, $n = 0$ being that of a plane wave. For symmetric flow about the centerplane of the channel only even values of n are admissible. As the frequency of oscillation σ is reduced, propagating modes of higher values of n begin to disappear successively and reemerge as decaying modes. The "cut-off frequency" of the n-th mode is

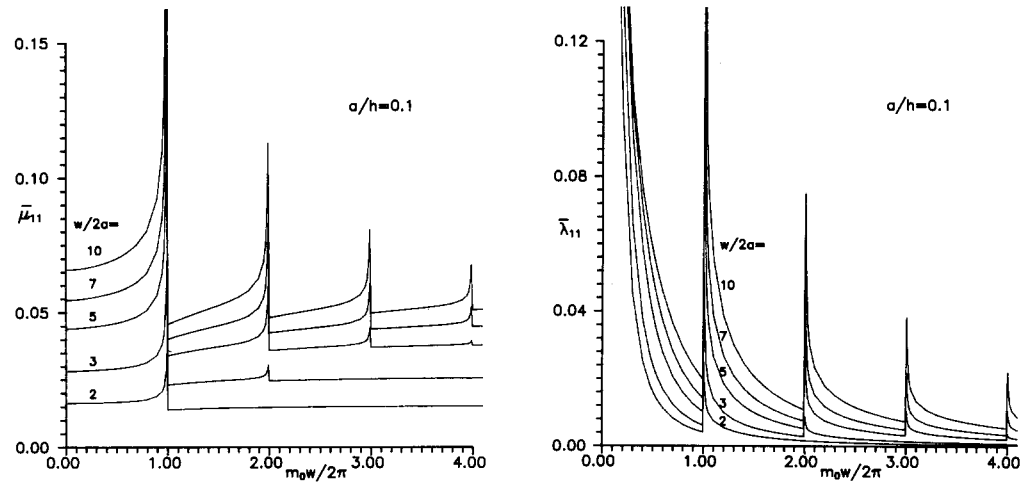

Fig. 3. (a) Nondimensional added-mass coefficient, equation (C.5), (b) nondimensional damping coefficient, equation (C.8), for surge motion of a flapper wavemaker, as a function of $m_0 w/(2\pi)$; $a/h = 0.1$, $w/(2a) = 2, 3, 5, 7$ and 10.

given by the vanishing of (3.1), or alternatively,

$$\frac{\sigma^2}{g} = \left(\frac{n\pi}{w}\right) \tanh\left(\frac{n\pi h}{w}\right) \quad \text{for } n = 2, 4, \ldots, \tag{3.2}$$

which coincides with the resonant frequencies for symmetric transverse oscillation of the channel. Figures 3a and 3b depict the added mass and damping, based on equations (C.5) and (C.8), respectively. It is evident from this analysis that a square-root singularity occurs at each integer value of $m_0 w/(2\pi)$. Further, because of the manner in which propagating modes "transform" to decaying modes around the cut-off, the damping coefficient of the wavemaker is singular at frequencies slightly above the cut-off value, whereas the added mass is singular at frequencies slightly below the cut-off.

Returning to the problem of vertical cylinders, we first present the results of (2.37) plotted against a nondimensional frequency based on the cylinder radius, $m_0 a$, which is proportional to the ratio of cylinder radius to the wavelength of a plane wave $\lambda_0 (= 2\pi/m_0)$ of the same frequency. Figures 4a and 4b are based on a geometric configuration of $d/a = 2$ and $a/h = 0.1$. The ratio of channel width to cylinder radius is shown as a parameter. Results for this graph as well as others reported below are based on $N = 7$ and $K = 7$ (i.e., 64 coupled coefficients) in (2.36). Comparing these new results with the case of a single cylinder ($w/(2a) = \infty$), we observe that the hydrodynamic properties are strongly influenced by the presence of the channel walls for wavelengths λ_0 longer than $\sim 6a$. For shorter waves (i.e., higher frequencies), the effects of the walls are negligible. Results in the presence of channel walls tend to oscillate about those of a single cylinder. The typical lower-frequency behavior is characterized by the presence of "spikes". Figures 5a and 5b show the same results plotted against a frequency parameter based on the channel width, $m_0 w/(2\pi)$, as in the case of the wavemaker solution. The behavior now resembles closely that of Figure 3a, b. It is evident that the occurrence of such spiky behavior is associated with the cut-off frequencies (3.2) discussed above. This is concomittantly related to the singular points of the series (2.26) and (B.6). It is also of interest to note that when the dimension of the cylinder is comparable to

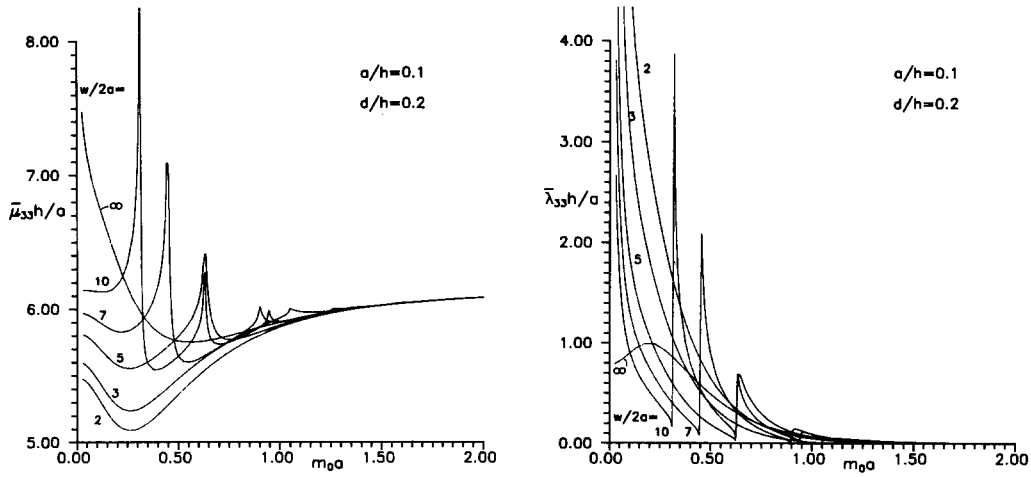

Fig. 4. (a) Nondimensional added-mass coefficient, (b) nondimensional damping coefficient for heave motion, as a function of m_0a; $a/h = 0.1$, $d/h = 0.2$, $w/(2a) = 2, 3, 5, 7, 10$ and θ.

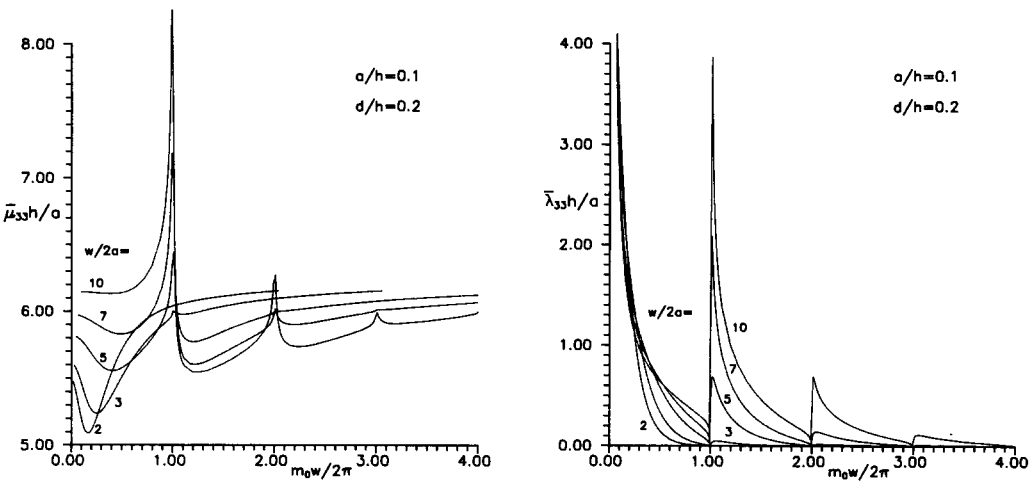

Fig. 5. (a) Nondimensional added-mass coefficient, (b) nondimensional damping coefficient for heave motion, as a function of $m_0w/(2\pi)$; $a/h = 0.1$, $d/h = 0.2$, $w/(2a) = 2, 3, 5, 7$ and 10.

the channel width, the resonant behavior is greatly inhibited, and finally disappears altogether (see e.g., $w/(2a) = 2$). The presence of a relatively large body has obviously destroyed the occurrence of transverse standing waves. The resonant modes are much more dominant when the body appears more like a point in the channel. This observation suggests that tank-test results, obtained with the purpose of simulating an open domain, must be interpreted with caution at the lower frequencies.

In the low-frequency range, the added mass and damping in a channel exhibit different limiting behavior from those of an open domain. From Yeung [1], the finite-depth added mass and damping coefficient of a *single* cylinder are known to be logarithmically singular and constant, respectively, in the limit of $\sigma \to 0$. The presence of the image array changes the behavior drastically. In this limit, the body and its image system appear together like a two-dimensional horizontal cylinder spanning across the width of the channel. The heave added mass and damping of two-dimensional cylinders in water of finite depth was a subject

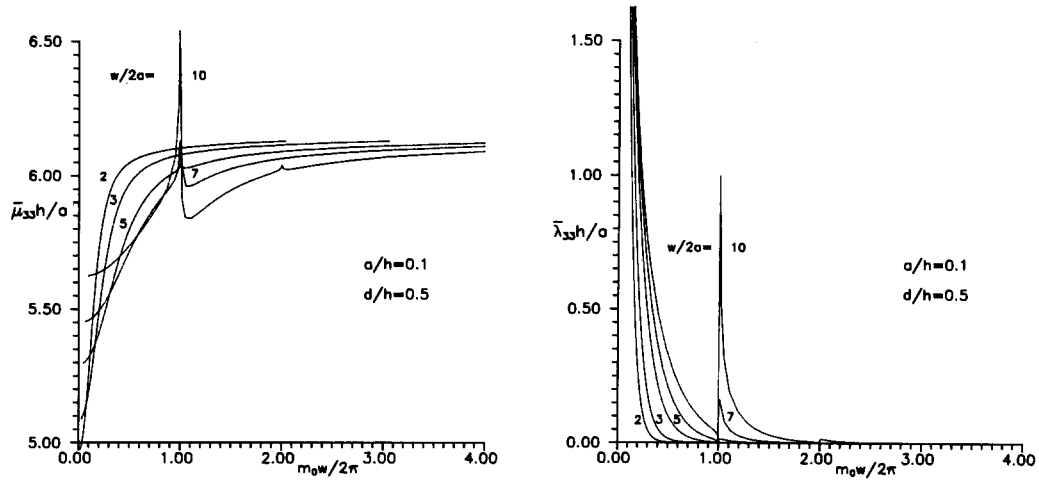

Fig. 6. (a) Nondimensional added-mass coefficient, (b) nondimensional damping coefficient for heave motion, as a function of $m_0 w/(2\pi)$; $a/h = 0.1$, $d/h = 0.5$, $w/(2a) = 2$, 3, 5, 7 and 10.

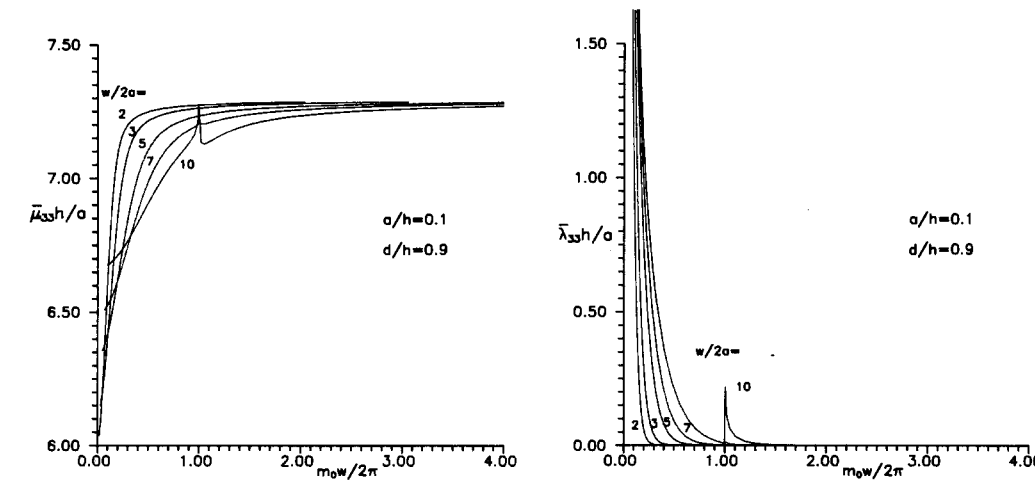

Fig. 7. (a) Nondimensional added-mass coefficient, (b) nondimensional damping coefficient for heave motion, as a function of $m_0 w/(2\pi)$; $a/h = 0.1$, $d/h = 0.9$, $w/(2a) = 2$, 3, 5, 7 and 10.

that received considerable attention in the mid-70's. Yeung and Newman [16] showed that, in this low-frequency limit, the added mass should approach a constant while the damping coefficient behaves like $(m_0 h)^{-1}$. The present low-frequency three-dimensional numerical results are observed to behave like those of two-dimensional horizontal cylinders.

Figures 6a and 6b show the heave results for a cylinder with a d/a ratio of 5. The corresponding results for the case of $d/a = 9$ are given in Figs. 7a and 7b. The basic features are similar to those of Fig. 5a, b. As the source of disturbance, i.e. the bottom of the cylinder, gets more submerged, wave effects, and hence the cut-off frequencies, become less prominent. As the gap between the bottom of the cylinder and the channel bottom is reduced, the added mass is also seen to rise rapidly. It is noteworthy that the actual fluid response at "cut-off" should be considered nonlinear and unsteady. Nonlinear behavior at cut-off is a subject of active investigation (see, e.g., Miles [18]).

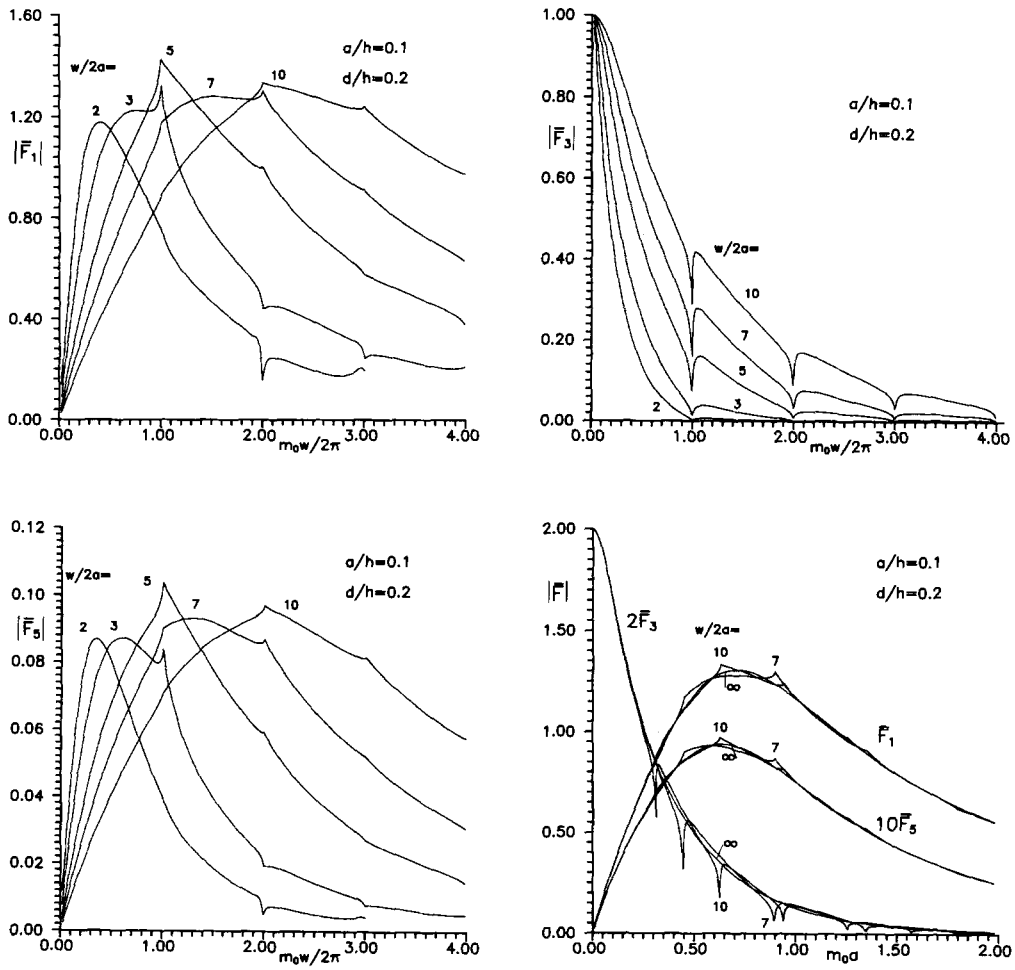

Fig. 8. Modulus of nondimensional wave-exciting force/moment: (a) horizontal, (b) vertical, (c) overturning moment, as a function of $m_0w/(2\pi)$, (d) as a function of m_0a; $a/h = 0.1$, $d/h = 0.2$, $w/(2a) = 2, 3, 5, 7$ and 10.

Figures 8a, 8b, and 8c display the wave-exciting horizontal and vertical forces, and the overturning moment on the cylinder respectively for the case of $d/h = 2$. All other parameters are kept the same as in the heave radiation study earlier. The general features of the force and moment are similar to those of a single cylinder of finite draft (Garrett [7]) with the exception of the occurrence of small spikes at the cut-off frequencies (see Fig. 8d). The spikes are generally not as pronounced as those of the radiation problem. A small instability exists in the matrix system of (2.43–44) at the higher cut-off frequency for the case of $w/(2a) = 2$. It is worthwhile to note that the vertical exciting force is more affected by the presence of channel walls than the horizontal force and turning moment. Since the exciting force/moment are related directly to the radiation damping of the corresponding mode, this behavior is considered plausible for the following reason. Heaving motion of the cylinder generates waves of about equal magnitude radiating in all angular directions, whereas surge and pitch motion (about the y-axis) would generate waves primarily in the x-direction. From physical consideration, it is clear that the latter two motions would experience less interference from channel walls. Finally, weaker singularities are expected to occur at the cut-offs for wave-exciting forces since these quantities are related to the square-root of radiation

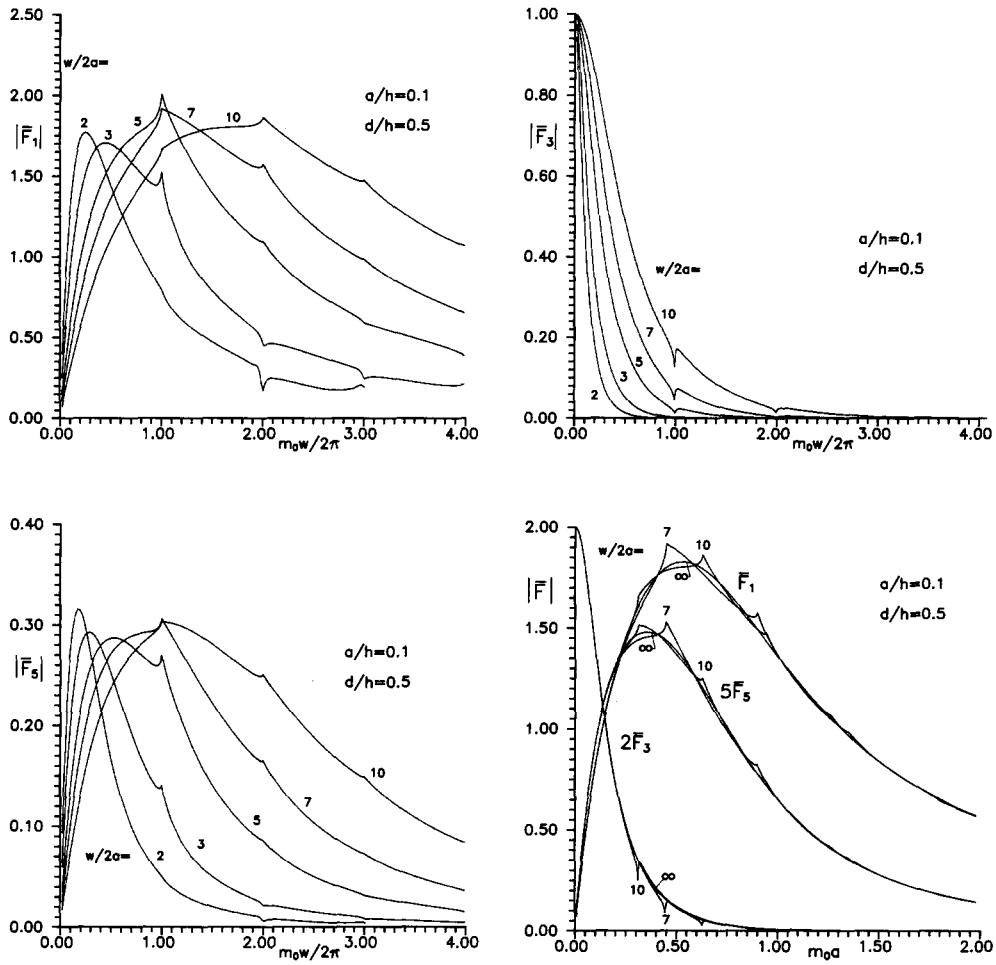

Fig. 9. Modulus of nondimensional wave-exciting force/moment: (a) horizontal, (b) vertical, (c) overturning moment, as a function of $m_0 w/(2\pi)$, (d) as a function of $m_0 a$; $a/h = 0.1$, $d/h = 0.5$, $w/(2a) = 2, 3, 5, 7$ and 10.

damping. This explains why the spikes are less pronounced in Fig. 8 when compared with Fig. 5. Figures 9a–d and Figs. 10a–d show results of similar trends for cylinders with deeper drafts.

4. Conclusions

The radiation and diffraction properties of a floating vertical cylinder of finite draft in a channel have been determined by the method of matched eigenfunction expansions. Wave effects on the central cylinder due to image cylinders associated with the channel walls are shown to be equivalent to a system of partial waves with angular variation. The magnitude of these angular modes are found to couple with the vertical modes under the cylinder. Numerical solution of a system of linear equations that couple the exterior and interior eigenfunction-expansion coefficients has been obtained.

The heave added mass and damping coefficient are found to be strongly influenced by the channel walls for wavelengths longer than approximately 6 times the cylinder radius. The

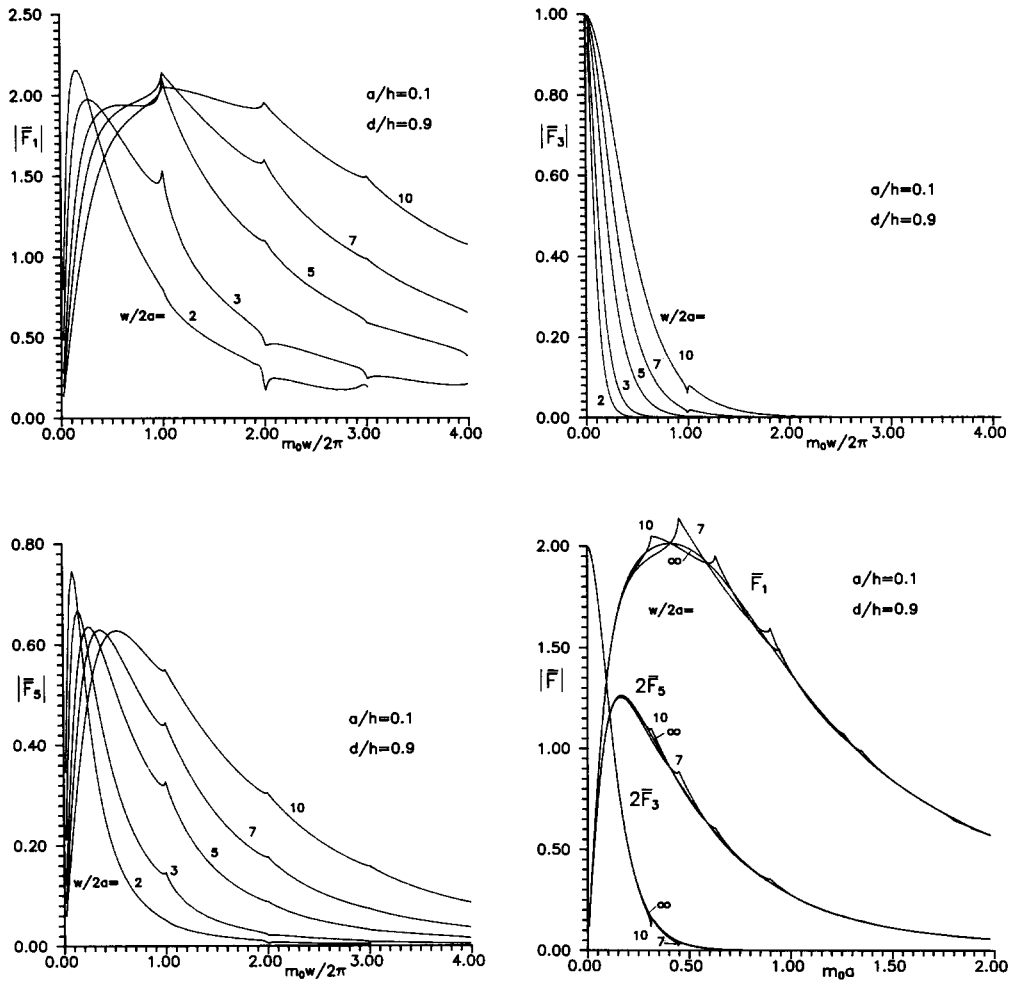

Fig. 10. Modulus of nondimensional wave-exciting force/moment: (a) horizontal, (b) vertical, (c) overturning moment, as a function of $m_0w/(2\pi)$, (d) as a function of m_0a; $a/h = 0.1$, $d/h = 0.9$, $w/(2a) = 2$, 3, 5, 7 and 10.

interference phenomenon manifests itself in the form of "spiky" responses at the cut-off frequencies of the channel. The cut-off frequencies are related to the occurrence of resonant transverse modes of oscillation symmetric about the channel centerline. A larger body, relative to the channel width, tends to suppress the magnitude of the "spikes" whereas a smaller body tends to accentuate them. At these lower frequencies, where interference is felt, both added mass and damping differ substantially from results for a single cylinder in a laterally unbounded fluid. However, such results tend to oscillate about the single-cylinder results as a mean.

The horizontal and vertical wave-exciting forces, as well as the overturning moment, acting on the cylinder due to unit-amplitude waves are also calculated. Similar interference effects are observed. The spiky behavior at the cut-off frequencies is not as pronounced as that of the radiation problem. Further, the horizontal force and pitching moment are found to be not as severely affected by the channel walls as the vertical force.

It is of interest to extend the present procedure to study the radiation properties associated with anti-symmetric motions, i.e., sway and roll. Based on the present study, one would

expect the "anti-symmetric cut-off frequencies" to play a dominant role in the hydrodynamic characteristics.

Acknowledgement

We are grateful for support provided in part by the Office of Naval Research (N00014-88-K0629) and in part by the University of California, under an internal grant. This work probably would not have been initiated were it not for the initial mention of the difficulties in obtaining reliable tank-test data for slow-drift motion by Dr S.L. Liou of Chevron Oil, California, and a Chevron research grant to the first author. We also acknowledge the Brazilian National Research Council for their sponsorship of S.H. Sphaier as a visiting scholar at Berkeley.

Appendix A: Application of Graff's addition theorem

Equation (2.21a) represents the summation of the influence of infinitely many cylinders on the left and right sides of the central cylinder. The Bessel functions have arguments expressed in terms of the local radius and the local polar angle of each cylinder. To transform the dependence of the many different radii and angles to the radius and angle relative the central cylinder, we apply Graff's addition theorem. It is established [11, p. 361] that

$$F_n(\Omega)e^{in\chi} = \sum_{p=-\infty}^{\infty} F_{n+p}(u)J_p(v)e^{ip\alpha} \tag{A.1}$$

where F_n denotes either J_n or Y_n, and Ω, χ, u, v, and α are defined with quotes in Fig. A.1.

For each pair of cylinders, one at each side and at the same distance from the central cylinder, we use the notation defined in Fig. A.1. Considering the cylinder on the left (+) side and right (−) side, from (A.1) we have

$$F_n(\Omega^{\pm})\cos n\theta_j = \sum_{p=-\infty}^{\infty} F_{n+p}(u^{\pm})J_p(v)\left[\left\{\cos\left(\frac{p\pi}{2}\right)\cos(p\theta_0) \mp \sin\left(\frac{p\pi}{2}\right)\sin(p\theta_0)\right\}\right.$$
$$\left.\times\cos\left(\frac{n\pi}{2}\right) + \left\{\sin\left(\frac{p\pi}{2}\right)\cos(p\theta_0) \pm \cos\left(\frac{p\pi}{2}\right)\sin(p\theta_0)\right\}\sin\left(\frac{n\pi}{2}\right)\right] \tag{A.2}$$

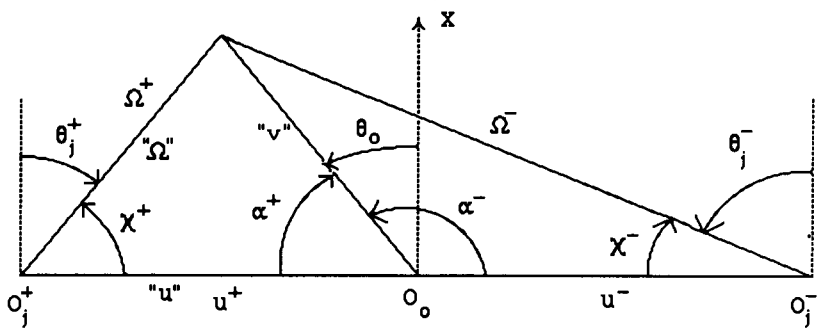

Fig. A.1. Nomenclature for Graff's theorem.

where $\alpha^{\pm} = \frac{1}{2}\pi \mp \theta_0$. Clearly, the cosine terms exist only for even values of n or p, the sine terms for odd values of n or p. Replacing u, v, and Ω by the arguments according to (2.21a),

$$\begin{aligned} u^{\pm} &= \pm jm_0 w \quad \text{for } j > 0, \\ v &= m_0 r_0, \\ \Omega^{\pm} &= m_0 r_j \qquad \text{for } j \neq 0, \end{aligned} \tag{A.3}$$

and combining contributions from the left and right cylinders, we observe the sine terms in the p series cancel in pair and the resulting expression is given by

$$\begin{aligned} &F_n(m_0 r_j^-) \cos(n\theta_j^-) + F_n(m_0 r_j^+) \cos(n\theta_j^+) \\ &= 2 \sum_{p=-\infty}^{\infty} F_{n+p}(jm_0 w) J_p(m_0 r_0) \cos(p\theta_0) \cos\left[(n-p)\frac{\pi}{2}\right] \end{aligned} \tag{A.4}$$

where only even values of n and p need to be kept.

Appendix B: Treatment of the Hankel-function series

The infinite series of Hankel functions shown in (2.26) is an alternating series with extremely slow convergence. If we subtract and add the leading-order asymptotic behavior of the Hankel functions from each term, the series in question can be rewritten as

$$\sum_{j=1}^{\infty} H_n^{(1)}(jx) = \sum_{j=1}^{\infty} \left[H_n^{(1)}(jx) - \sqrt{\frac{2}{\pi x}}\, e^{-i(n(\pi/2)+(\pi/4))} \frac{e^{ijx}}{\sqrt{j}} \right] + \sqrt{\frac{2}{\pi x}}\, e^{-i(n(\pi/2)+(\pi/4))} \sum_{j=1}^{\infty} \frac{e^{ijx}}{\sqrt{j}}. \tag{B.1}$$

Now the quantity in brackets of the first sum decays at a favorable rate of $j^{-3/2}$. In fact, using the asymptotic series of $H_n^{(1)}(x)$, the j-th term in the first series of (B.1) can be calculated to a very high degree of accuracy:

$$\begin{aligned} [\ldots]_j &= \frac{e^{i(jx - \pi/2(n-1/2))}\left(\frac{1}{4} - n^2\right)}{\sqrt{2\pi x^3}} \\ &\quad \times \left\{ -\frac{i}{j^{3/2}} + \left(\frac{9}{4} - n^2\right)\left[-\frac{1}{2xj^{5/2}} + (25 - n^2)\left[\frac{i}{4x^2 j^{7/2}} + \ldots \right] \right] \right\}. \end{aligned} \tag{B.2}$$

The second series in (B.1) turns out to be expressible in an integral form, which facilitates numerical treatment. From Gradshteyn and Ryzhik [19, p. 326],

$$\sum_{j=1}^{\infty} \frac{e^{ijx}}{j^{1/2}} = \frac{e^{ix}}{\sqrt{\pi}} \int_0^{\infty} y^{-1/2} [e^y - e^{ix}]^{-1}\, dy \equiv \frac{2}{\sqrt{\pi}} Q(x). \tag{B.3}$$

This expression was also used by Matsui et al. [13] but with no details given concerning the treatment of the integral $Q(x)$. A straight-forward change of variable yields

$$Q(x) = \int_0^\infty dy\ (e^{y^2+ix} - 1)/f(y) \tag{B.4a}$$

$$= e^{ix}A(x) - B(x) \tag{B.4b}$$

with

$$f(y) = e^{2y^2} - (2\cos x)e^{y^2} + 1. \tag{B.5}$$

The indeterminate form near $y = 0$ in (B.4a) requires some care in numerical integration. Asymptotic analysis of (B.4a) for small y at the singular points of $x = 2p\pi$, p being a positive integer, shows that

$$Q(x) \sim \alpha(x)/|x - 2p\pi|^{1/2} \tag{B.6}$$

where $\alpha(x)$ is regular in x. For sufficiently large values of y, it is clear that both $A(x)$ and $B(x)$ in (B.4b) have rapidly decaying integrands. If $f(y)$ in (B.5) is replaced by e^{2y^2}, which has an absolute error of the order of 10^{-36} for $y = 6$, the truncation errors E_A and E_B of the integrals A and B satisfy:

$$|E_B| < |E_A| \cong \int_{y_0}^\infty \frac{dy}{\exp(2y^2)} = \sqrt{\frac{\pi}{2}}\,\mathrm{erfc}\,(y_0), \tag{B.7}$$

where erfc is the complementary error function. For a value of $y_0 = 6$, E_A is thus of the order of 10^{-14}.

Appendix C: Solution for a flapper wavemaker

Consider a wavemaker with vertical flappers hinged at the axes $y = \pm a$ as shown in Fig. C.1. Let the displacement of the points on the plane of symmetry be given by $\zeta(t) = \zeta_1 \exp(-i\sigma t)$, where ζ_1 is the amplitude. The velocity potential can be written in relatively standard Cartesian eigenfunctions [20],

$$\phi = \mathrm{Re}\left\{-i\sigma\zeta_1 e^{-i\sigma t}\sum_{n=0}^{\infty}\sum_{k=0}^{\infty}\varepsilon_n a_{kn}F_{kn}(m_k, \beta_n)G_n(\beta_n y)Z_k^{(e)}(m_k z)\right\}, \tag{C.1a}$$

where

$$G_n(\beta_n y) = \cos[\beta_n(y - w/2)], \quad \beta_n = n\pi/w,$$

$$F_{kn}(m_k, \beta_n) = \begin{cases} e^{i\alpha_{0n}x}, & k = 0, \quad \alpha_{0n}^2 = m_0^2 - \beta_n^2 > 0, \\ e^{-\alpha_{0n}x}, & k = 0, \quad \alpha_{0n}^2 = \beta_n^2 - m_0^2 > 0, \\ e^{-\alpha_{kn}x}, & k \neq 0, \quad \alpha_{kn}^2 = m_k^2 + \beta_n^2. \end{cases} \tag{C.1b}$$

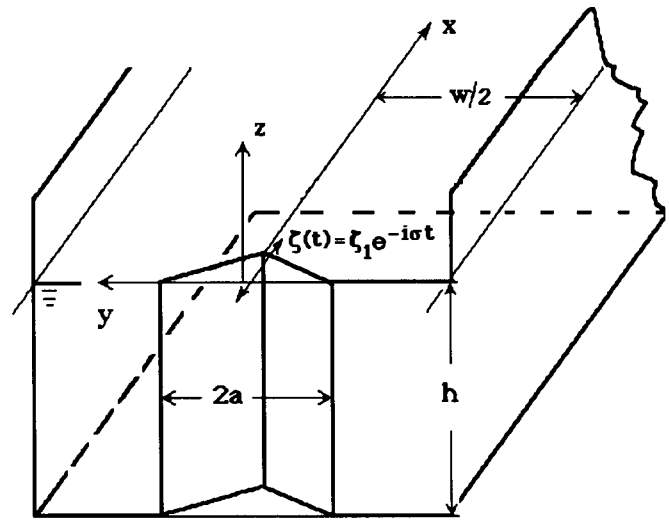

Fig. C.1. A wavemaker with vertical flapper.

Assuming small motions, $\zeta_1/a \ll 1$, we have the following linearized condition on the plane $x = 0$:

$$\frac{\partial \phi}{\partial n} \approx \frac{\partial \phi}{\partial x} = \text{Re}\,\{-g(y)i\sigma\zeta_1 e^{-i\sigma t}\}, \tag{C.2}$$

where

$$g(y) = \begin{cases} (a - |y|)/a & \text{for } |y| < a, \\ 0 & \text{for } a < |y| < w/2. \end{cases}$$

Using the eigenfunctions $Z_k^{(e)}$ and G_n, we can define an operator similar to (2.29) for the z- and y-integration. Application of such an operator to (C.2) using (C.1) yields the following expression for the coefficients of the eigenexpansions:

$$a_{qp} = f_q(m_q h)\gamma_p N_q^{-1/2}\left(\frac{\partial F_{qp}}{\partial x}\right)^{-1} \tag{C.3}$$

with

$$\gamma_0 = a/w, \quad \gamma_p = 0, \quad \text{for } p = \text{odd},$$

$$\gamma_p = \frac{2w}{a}(-1)^{p/2}\left[1 - \cos\left(\frac{p\pi a}{w}\right)\right]\Big/(p\pi)^2, \quad \text{for } p = 2, 4, \ldots .$$

Introducing (C.3) in (C.1), we can determine the hydrodynamic pressure acting on the wavemaker surface. Integrating this pressure we can obtain the component of the hydrodynamic

force in the x-direction:

$$\bar{F}_1 = \frac{F_1}{\varrho a h^2} = \frac{1}{ah^2}\int_{\mathscr{S}} \frac{\partial \phi}{\partial t}\,\mathrm{d}\mathscr{S} = -(\bar{\mu}_{11} + \mathrm{i}\bar{\lambda}_{11})\dot{\bar{\zeta}} = -\frac{1}{\varrho a h^2}\left(\mu_{11} + \frac{\mathrm{i}}{\sigma}\lambda_{11}\right)\dot{\zeta}, \quad \text{(C.4)}$$

where

$$\bar{\mu}_{11} = \bar{\mu}_{110} + \bar{\mu}_{11c}, \quad \text{(C.5)}$$

$$\bar{\mu}_{110} = \frac{2}{\pi^4}\frac{w^3}{ha^2}\frac{\sinh(m_0 h)}{N_0(m_0 h)^2}\sum_{p=P+1}^{\infty}\frac{\sin(\beta_p a)[1-\cos(\beta_p a)]}{p^3\sqrt{\left(\frac{p}{2}\right)^2 - \left(\frac{m_0 w}{2\pi}\right)^2}}, \quad \text{(C.6)}$$

$$\bar{\mu}_{11c} = \frac{2w}{a}\sum_{k=1}^{\infty}\frac{\sin(m_k h)}{N_k(m_k h)^2}\left\{\frac{a^2}{w^2}\frac{1}{m_0 h} + \frac{w^2}{ah}\frac{1}{\pi^4}\sum_{p=2,4\ldots}^{\infty}\frac{\sin(\beta_p a)[1-\cos(\beta_p a)]}{p^3\sqrt{\left(\frac{p}{2}\right)^2 + \left(\frac{m_k w}{2\pi}\right)^2}}\right\}, \quad \text{(C.7)}$$

and

$$\bar{\lambda}_{11} = \frac{2w}{a}\frac{\sinh^2(m_0 h)}{N_0(m_0 h)^2}\left\{\frac{a^2}{w^2}\frac{1}{m_0 h} + \frac{w^2}{ah}\frac{1}{\pi^4}\sum_{p=2,4\ldots}^{P}\frac{\sin(\beta_p a)[1-\cos(\beta_p a)]}{p^3\sqrt{\left(\frac{m_0 w}{2\pi}\right)^2 - \left(\frac{p}{2}\right)^2}}\right\}. \quad \text{(C.8)}$$

Here, in accordance with (C.1b), P is the largest value of p satisfying $p < (m_0 w)/\pi$. Individual contributions by the propagating and decaying modes to the added mass are shown explicitly in (C.6) and (C.7). Note the occurrence of a square-root infinity as $m_0 w$ approaches an (integer) value of p. The "bandwidth" of the singularity decreases with increasing p. The decaying modes do not generate any discontinuous behavior at these so-called "cut-off" frequencies. The damping coefficient, on the other hand, exhibits such a singular behavior at frequencies slightly above the cut-off.

The energy flux across a plane normal to the x-axis is intimately related to the damping. A time-averaged nondimensional energy flux can be derived and is given by

$$\bar{\mathscr{F}} = \frac{1}{\frac{1}{2}\varrho(\sigma\zeta_1)^2 h^2 a\sigma}\frac{1}{T}\varrho\int_0^T\int_{-w/2}^{w/2}\int_{-h}^{0}\frac{\partial\phi}{\partial x}\frac{\partial\phi}{\partial t}\,\mathrm{d}z\,\mathrm{d}y\,\mathrm{d}t$$

$$= \frac{1}{\pi}\frac{w}{2a}\frac{w}{h}\frac{\sinh^2(m_0 h)}{N_0(m_0 h)^2}\left[\left(\frac{a}{w}\right)^2\frac{2\pi}{m_0 w} + \sum_{p=2,4\ldots}^{P}\frac{4w^2}{(p\pi)^4 a^2}\frac{(1-\cos(\beta_p a))^2}{\sqrt{\left(\frac{m_0 w}{2\pi}\right)^2 - \left(\frac{p}{2}\right)^2}}\right], \quad \text{(C.9)}$$

which shows that large damping is associated with the generation of large-amplitude waves near the resonant frequencies of the transverse modes of oscillation of the channel. Equations (C.5) and (C.8) are shown in Figs. 3a and 3b. It is interesting to note that as the flapper width 2a approaches the channel width, cut-off frequencies exist only at $(m_0 w)/\pi = 2, 6, 10, \ldots$.

References

1. Yeung, R.W., Added mass and damping of a vertical cylinder in finite-depth waters, *Applied Ocean Research* 3 (1981) 119–133.
2. Simon, M.J., Multiple scattering in arrays of axisymmetric wave-energy devices, Part 1: A matrix method using a plane-wave approximation, *J. Fluid Mech.* 120 (1982) 1–25.
3. McIver, P. and Evans, D.V., Approximation of wave forces on cylinder arrays, *Applied Ocean Research*, 6 (1984) 101–107.
4. Mavrakos, S.A. and Koumoutsakos, P., Hydrodynamic interaction among vertical axisymmetric bodies restrained in waves, *Applied Ocean Research*, 9 (1987) 128–140.
5. Zhao, R., Faltinsen, O., Krokstad, J. R. and Aanesland, V., Wave-current interaction effects on large-volume structures, *Proceedings BOSS Conference* (1988) Trondheim, Norway.
6. Bai, K.J., Diffraction of oblique waves by an infinite cylinder, *J. Fluid Mech.* 68 (1975) 513–535.
7. Garrett, C.J.R., Wave forces on a circular dock, *J. Fluid Mech.* 46 (1971) 129–139.
8. Miao, G. P. and Liu, Y.Z., Hydrodynamical coefficients of a column with footing in finite-depth waters, *Proc. 3rd Int. OMAE Symp. ASME*, New Orleans, Louisiana, 1 (1984) 199–205.
9. McIver, P., Wave forces on adjacent floating bridges, *Applied Ocean Research* 8 (1986) 67–75.
10. Kagemoto, H. and Yue, D.K.P., Interactions among multiple three-dimensional bodies in water waves: an exact algebraic method, *J. Fluid Mech.* 166 (1986) 189–209.
11. Watson, G.N., *A Treatise on the Theory of Bessel Functions*, Cambridge University Press (1944).
12. Spring, B.W. and Monkmeyer, P.L., Interaction of plane waves with a row of cylinders, *Proceedings 3rd Conf. Civil Engg. in Oceans, ASCE*, Newark, Del. (1975) 979–998.
13. Matsui, T., Shirai, T., Sugita, H., Ohmori, H., Endo, M. and Ohki, K., Slowly varying wave drift forces on an articulated column; 2nd report: experiment in regular waves, *J. Soc. of Naval Architects of Japan* 160 (1986) 185–194.
14. Twersky, V., Multiple scattering of radiation by an arbitrary configuration of parallel cylinders, *J. Acoustical Soc. of America* 24 (1952) 42–46.
15. Bai, K.J. and Yeung, R.W., Numerical solution to free-surface flow problems, *Proceedings 10th Symp. Naval Hydrodynamics*, Cambridge, Mass. (1974) 609–647.
16. Yeung, R.W. and Newman, J.N., Discussion paper on Paper by Sayer, P. and Ursell, F.: On the virtual mass, at long wavelengths, of a half-immersed circular cylinder heaving on water of finite depth, *Proceedings 11th Symp. Naval Hydrodynamics*, London (1976) 560–561.
17. Thomas, G.P., The diffraction of water waves by a circular cylinder in a channel, *Abstract for the 2nd International Workshop on Water Waves and Floating Bodies*, Bristol, England (March 1987).
18. Miles, J., Guided surface waves near cut-off, *J. Fluid Mech.* 189 (1988) 287–300.
19. Gradshteyn, I.S. and Ryzhik, I.M., *Table of Integrals, Series and Products*, New York, Academic Press (1965).
20. Wehausen, J.V. and Laitone, E., Surface waves, *Handbuch der Physik*, Berlin, Springer Verlag, Vol. IX (1960) 474.